



Cite this: DOI: 10.1039/d4cc01414f

Received 28th March 2024,
Accepted 5th June 2024

DOI: 10.1039/d4cc01414f

rsc.li/chemcomm

Cooperative defect engineering and ligand modification in UiO-66 to achieve high proton conductivity†

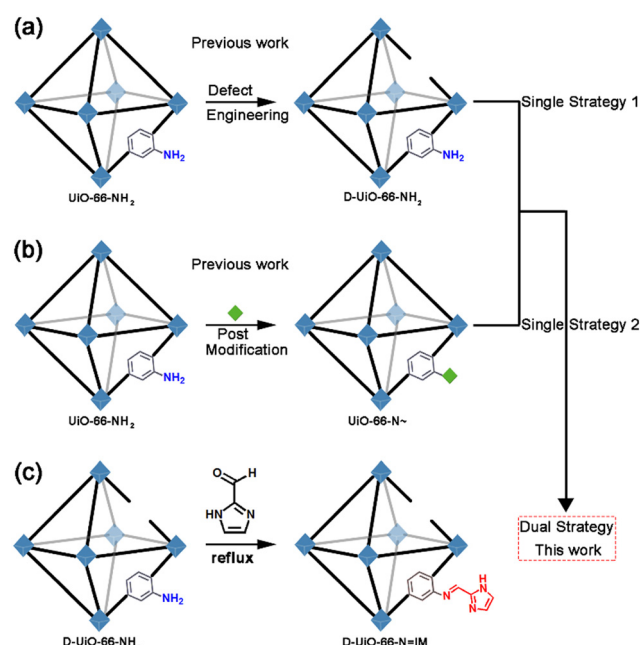
Xiao-Min Li,^{‡a} Junchao Jia,^{‡a} Mingyang Zhao,^a Dongbo Liu,^a Junkuo Gao^{id}*^a and Ya-Qian Lan^{id}*^b

D-UiO-66-N=IM with high proton conductivity has been synthesized through the dual strategy of defect engineering and ligand modification. Moreover, D-UiO-66-N=IM exhibits good temperature cycling stability and durability in proton conductivity. This work has developed a new method to obtain efficient MOF-based proton conductors.

The global energy consumption and environmental pollution caused by the excessive use of fossil fuels are becoming increasingly serious. In order to address carbon emissions and climate change, efforts towards the global energy structure transformation from fossil fuels to renewable and clean energy are being implemented.^{1–3} The proton exchange membrane fuel cell (PEMFC) has emerged as an alternative to traditional engines because of its high energy density and pollution-free characteristics.^{4,5} However, achieving widespread commercialization of PEMFCs still faces many challenges, such as reducing costs, increasing power density, and improving stability and durability.^{6,7} As the core component of PEMFCs, the PEM needs to be optimized from various aspects. Currently, Nafion is the most widely used electrolyte membrane, but its disordered structure limits the precise analysis of the proton conduction mechanism.⁸ Moreover, the strong hydrophilicity of sulfonic acid groups in Nafion can cause it to swell.^{9,10} Therefore, developing electrolyte materials with a defined structure and structural stability is necessary and meaningful.

Metal-organic frameworks (MOFs) are considered potential materials for exploring proton conductors due to their clear structures and functional frameworks.² The clear structural information of MOFs plays a promoting role in understanding

the proton conduction mechanism.¹¹ On the other hand, the functionalized framework of MOFs provides the possibility for the directed synthesis of a stable proton conductor with high proton conductivity.¹² Currently, there are three design strategies for MOF-based proton conductors. Firstly, encapsulating small molecules that can serve as proton carriers in MOF pores to promote proton transport.^{13–15} Secondly, utilizing defect engineering in MOFs to increase acidic centers of the frameworks to enhance proton mobility (Scheme 1a).^{16,17} Thirdly, utilizing the functionalization of MOF frameworks to



Scheme 1 (a) Schematic diagram of using defect engineering of MOFs to prepare a proton conductor in previous work. (b) Schematic diagram of using post-modification of MOFs to prepare a proton conductor in previous work. (c) Schematic diagram of using the dual strategy to prepare a proton conductor in this work.

^a Institute of Functional Porous Materials, School of Materials Science and Engineering, Zhejiang Sci-Tech University, Hangzhou 310018, P. R. China. E-mail: jkgao@zstu.edu.cn

^b School of Chemistry, South China Normal University, Guangzhou, Guangdong 510006, P. R. China. E-mail: yqlan@m.scnu.edu.cn

† Electronic supplementary information (ESI) available. See DOI: <https://doi.org/10.1039/d4cc01414f>

‡ These authors contributed equally to this work.

post-modify metal centers or organic ligands to form stable proton conductors with high proton conductivities (Scheme 1b).^{18–20} Previous studies have focused on a single strategy. There is limited research on developing efficient proton conductors using dual strategies.

Herein, we have developed a dual strategy that combines defect engineering and framework post-modification of MOFs to prepare **D-UiO-66-N=IM** (Scheme 1c). Firstly, UiO-66-NH₂ with defective sites (D-UiO-66-NH₂) was synthesized. The method of causing partial ligand deficiency in UiO-66-NH₂ is a mature, simple, and low-cost technology. The formation of D-UiO-66-NH₂ can increase the acidic center to enhance proton mobility. Subsequently, 1*H*-imidazole-2-carbaldehyde was selected to react with D-UiO-66-NH₂ through a Schiff base reaction to generate **D-UiO-66-N=IM**. The introduction of imidazole groups can increase proton sources and proton hopping sites. **D-UiO-66-N=IM** exhibited a high proton conductivity of 2.15×10^{-2} S cm⁻¹ at 70 °C and 100% relative humidity (RH). Moreover, **D-UiO-66-N=IM** exhibited good performance in terms of cycling stability and durability.

D-UiO-66-NH₂ and **D-UiO-66-N=IM** were synthesized. Meanwhile, we synthesized UiO-66-N=IM by reacting UiO-66-NH₂ with 1*H*-imidazole-2-carboxaldehyde as a control sample. As can be seen in Fig. 1a, the PXRD patterns of D-UiO-66-NH₂, UiO-66-N=IM, and **D-UiO-66-N=IM** are basically identical to that of the simulated UiO-66, proving that their UiO-66 frameworks have been preserved. The successful post-modification of UiO-66-N=IM and **D-UiO-66-N=IM** can be verified through FTIR spectra (Fig. 1b). Compared to the vibrational bands of -NH₂ groups located at 3587 cm⁻¹ and 1650 cm⁻¹ in D-UiO-66-NH₂, those in UiO-66-N=IM and **D-UiO-66-N=IM** have disappeared due to the Schiff base reaction.^{21,22} In addition, there are new peaks located at 2931 cm⁻¹, 1654 cm⁻¹, and 1097 cm⁻¹ in the spectra of UiO-66-N=IM and **D-UiO-66-N=IM**, which are attributed to -N-H, -C=N, and -C-N groups, respectively. These peaks indicate the

successful occurrence of the Schiff base reaction.^{22–24} The decreasing N₂ adsorption capacities of UiO-66-N=IM and **D-UiO-66-N=IM** manifest that 1*H*-imidazole-2-carboxaldehyde has been grafted onto their frameworks (Fig. S1, ESI†). Additionally, the N₂ adsorption capacity of **D-UiO-66-N=IM** is smaller than that of UiO-66 due to the presence of functionalized molecules in the pores of **D-UiO-66-N=IM**. The results of dissolution/¹H NMR spectra of D-UiO-66-NH₂ and **D-UiO-66-N=IM** show that there are new resonances of H_d, H_e, and H_f, confirming the presence of alkene protons and formation of imine groups (Fig. S2, ESI†).^{22,23,25–27} It can be calculated that the number of imidazole units introduced in a D-UiO-66-NH₂ unit is 1.2. The defect engineering in D-UiO-66-NH₂ was confirmed through various characterizations. UiO-66-NH₂ was also synthesized as a reference material (Fig. S3, ESI†). Firstly, the thermogravimetric analysis (TGA) curves of UiO-66-NH₂ and D-UiO-66-NH₂ were measured (Fig. 1c). The weight loss that occurs within the temperature range of room temperature to ~350 °C is due to water molecules and acetic acid molecules.²⁸ The frameworks of UiO-66-NH₂ and D-UiO-66-NH₂ can remain stable until ~500 °C. Their final residue is ZrO₂, the weight of which is normalized to 100%. The final weight loss is organic linker loss.^{29,30} It can be observed that the weight loss of organic linkers in UiO-66-NH₂ is greater than that in D-UiO-66-NH₂, indicating the presence of defect sites in D-UiO-66-NH₂. Secondly, the N₂ adsorption capacity and pore size distribution of UiO-66-NH₂ and D-UiO-66-NH₂, as obtained from N₂ adsorption measurements, also demonstrate the presence of defect sites introduced by the acetic acid modulator in D-UiO-66-NH₂, because more pore sizes exist in D-UiO-66-NH₂ (Fig. S4 and S5, ESI†). Thirdly, the dissolution/¹H NMR spectra of UiO-66-NH₂ and D-UiO-66-NH₂ were collected, from which it can be observed that an additional signal peak corresponding to the acetic acid modulator in D-UiO-66-NH₂ is present compared to that in UiO-66-NH₂ (Fig. S6, ESI†).³⁰ Moreover, we employed the common acid–base titration method to determine the missing linker number in D-UiO-66-NH₂ (Fig. 1d). It can be calculated that the number of missing linkers in D-UiO-66-NH₂ is 0.74. (A detailed procedure can be found in the ESI†) These results demonstrate that D-UiO-66-NH₂ has been successfully fabricated.

The morphology and other physical properties of D-UiO-66-NH₂, UiO-66-N=IM, and **D-UiO-66-N=IM** have also been characterized. As shown in Fig. S7–S9 (ESI†), the octahedral structure of UiO-66 was preserved, consistent with the findings from the PXRD patterns of D-UiO-66-NH₂, UiO-66-N=IM, and **D-UiO-66-N=IM**. The energy-dispersive X-ray (EDX) spectra of D-UiO-66-NH₂, UiO-66-N=IM, and **D-UiO-66-N=IM** show the presence of elements C, N, O, and Zr (Fig. S10–S12, ESI†). Accompanied by the EDX spectra, their EDX maps were scanned, and the same results as those in the EDX spectra were obtained (Fig. S13–S15, ESI†). To assess the thermal stability of D-UiO-66-NH₂, UiO-66-N=IM, and **D-UiO-66-N=IM**, their TGA curves were analyzed. It can be seen from Fig. S16–S18 (ESI†) that the three materials exhibit sufficient thermal stability for proton conductivity tests.

In order to verify the advantages of the dual strategy in improving proton conductivity, we conducted AC impedance

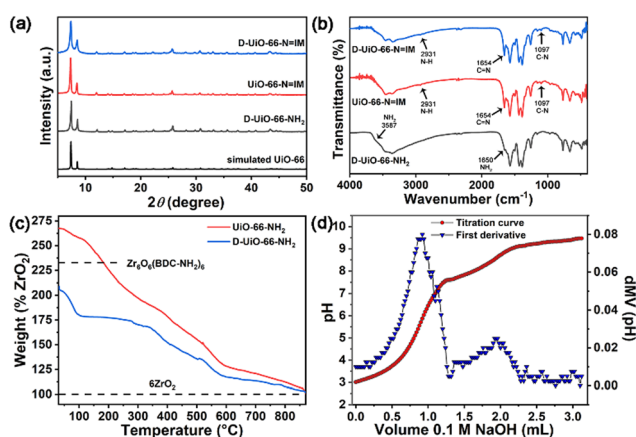


Fig. 1 (a) PXRD patterns of simulated UiO-66 (black), as-synthesized D-UiO-66-NH₂ (gray), as-synthesized UiO-66-N=IM (red) and as-synthesized **D-UiO-66-N=IM** (blue). (b) FTIR spectra of as-synthesized D-UiO-66-NH₂ (gray), UiO-66-N=IM (red) and **D-UiO-66-N=IM** (blue). (c) TGA curves of as-synthesized UiO-66-NH₂ (red) and as-synthesized D-UiO-66-NH₂ (blue). The end weight of ZrO₂ is normalized to 100%. (d) Acid–base titration curve and first derivative curve for D-UiO-66-NH₂.

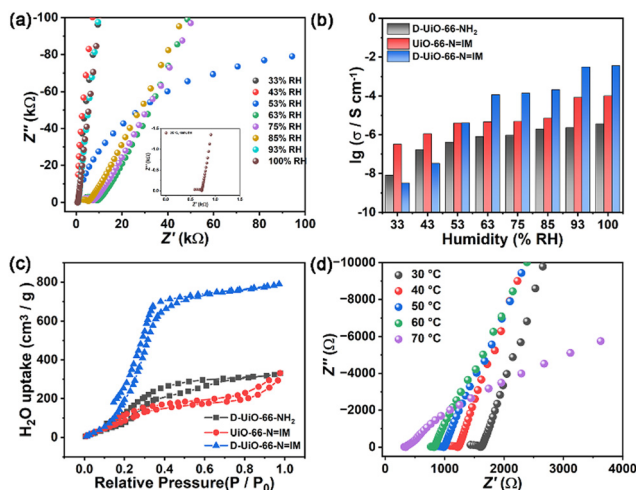


Fig. 2 (a) Nyquist plots of **D-UiO-66-N=IM** at room temperature and different humidities varying from 33% to 100% RH. Inset is the Nyquist plot of **D-UiO-66-N=IM** at room temperature and 100% RH. (b) Proton conductivities of **D-UiO-66-NH₂** (gray), **UiO-66-N=IM** (red) and **D-UiO-66-N=IM** (blue) at room temperature and different humidities varying from 33% to 100% RH. (c) Water sorption isotherms of **D-UiO-66-NH₂** (gray), **UiO-66-N=IM** (red) and **D-UiO-66-N=IM** (blue) at 298 K. (d) Nyquist plots of **D-UiO-66-N=IM** at 100% RH and different temperatures varying from 30 to 70 °C.

spectroscopy tests on **D-UiO-66-NH₂**, **UiO-66-N=IM**, and **D-UiO-66-N=IM**. Firstly, their proton conductivities were measured at room temperature and different humidities ranging from 33% to 100% (Fig. S19 and S20, ESI† and Fig. 2a). The Nyquist plots display high-frequency arcs and low-frequency tails, which correspond to the bulk and grain resistances, and moving ion resistance, respectively.³¹ As can be seen in Fig. 2b, the proton conductivities of **D-UiO-66-NH₂**, **UiO-66-N=IM**, and **D-UiO-66-N=IM** increase with increasing humidity. Notably, the proton conductivities of **D-UiO-66-NH₂** and **UiO-66-N=IM** are higher than that of **D-UiO-66-N=IM** under low humidity conditions (33% and 43% RH). This difference may be attributed to the single proton transport pathway in the larger pores of **D-UiO-66-NH₂**, which plays a significant role in proton conductivity in the former case, while the presence of more post-modified molecules in **UiO-66-N=IM** has a major impact on proton conductivity in the latter case. Quickly, the advantages of the dual strategy become apparent. As the humidity continues to rise, the proton conductivities of **D-UiO-66-N=IM** are much higher than those of **D-UiO-66-NH₂** and **UiO-66-N=IM** due to the positive cooperative impact of defect engineering and ligand modification. The missing linker in **D-UiO-66-NH₂** can increase acidic centers to enhance proton mobility. The imidazole groups introduced into **D-UiO-66-N=IM** contain proton sources and proton hopping sites, which are beneficial for proton conduction. At room temperature and 100% RH, the proton conductivities of **D-UiO-66-NH₂**, **UiO-66-N=IM**, and **D-UiO-66-N=IM** are $3.66 \times 10^{-6} \text{ S cm}^{-1}$, $1.03 \times 10^{-4} \text{ S cm}^{-1}$ and $3.53 \times 10^{-3} \text{ S cm}^{-1}$, respectively. It can be observed from the water sorption isotherms of **D-UiO-66-NH₂**, **UiO-66-N=IM**, and **D-UiO-66-N=IM** at 298 K that **D-UiO-66-N=IM** has the highest

water adsorption capacity, which is advantageous for effective proton transport (Fig. 2c).

To assess the impact of temperature on proton conduction, the temperature-dependent proton conductivities of **D-UiO-66-NH₂**, **UiO-66-N=IM**, and **D-UiO-66-N=IM** at 100% RH were measured (Fig. S21 and S22, ESI† and Fig. 2d). Similarly, temperature plays a positive role in proton conductivity. It can be calculated that the proton conductivities of **D-UiO-66-NH₂**, **UiO-66-N=IM**, and **D-UiO-66-N=IM** at 70 °C and 100% RH are $6.18 \times 10^{-4} \text{ S cm}^{-1}$, $7.48 \times 10^{-4} \text{ S cm}^{-1}$, and $2.15 \times 10^{-2} \text{ S cm}^{-1}$, respectively. The proton conductivity of **D-UiO-66-N=IM** is nearly two orders of magnitude higher than that of **D-UiO-66-NH₂** and **UiO-66-N=IM**, and can be comparable to the performance of Nafion ($10^{-2} \text{ S cm}^{-1}$).³² This improvement is attributed to the synergistic effect of increased acidic centers resulting from defect engineering, increased proton carriers from the post-modified molecule, and the presence of abundant water molecules from the humidifier. In addition, the activation energy (E_a) values were obtained from the Arrhenius plots. The E_a values of **D-UiO-66-NH₂**, **UiO-66-N=IM**, and **D-UiO-66-N=IM** are 0.50 eV, 0.30 eV, and 0.38 eV, respectively (Fig. S23–S25, ESI†). The results indicate that proton conduction in **D-UiO-66-NH₂** follows a vehicle mechanism, while proton conduction in **UiO-66-N=IM** and **D-UiO-66-N=IM** is attributed to the Grotthuss mechanism. This finding is consistent with their respective proton conductivities.

In order to intuitively determine the proton conduction performance of **D-UiO-66-N=IM** in MOF-based proton conductors, a comparison is summarized based on the preparation strategy as the classification criterion (Fig. 3a). The specific information is shown in Table S1 (ESI†). It can be seen that the proton conductivity of **D-UiO-66-N=IM** prepared through the dual strategy exceeds

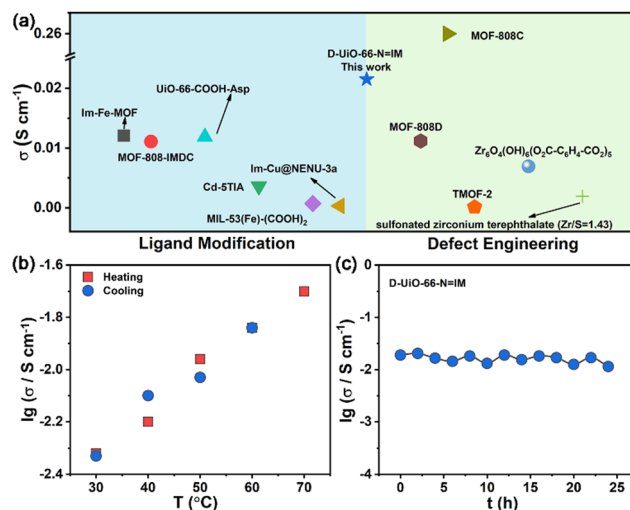


Fig. 3 (a) Comparison of proton conductivities and preparation strategies of **D-UiO-66-N=IM** and some other representative MOF-based proton conductors measured under hydrous conditions. (b) Proton conductivities for the heating-cooling cycle of **D-UiO-66-N=IM** in the temperature range of 30–70 °C and 100% RH. (c) The time-dependent proton conductivities of **D-UiO-66-N=IM** measured at 70 °C and 100% RH.

that of the majority of MOF-based proton conductors using a single preparation strategy. Notably, the proton conductivity of MOF-808C is higher than that of **D-UiO-66-N=IM**. The pore size and volume of MOF-808 are larger than those of UiO-66, which may lead to defective MOF-808 having more acidic centers and stronger ability to accommodate water molecules, resulting in higher proton conductivity. Furthermore, to evaluate the practical application potential of **D-UiO-66-N=IM**, its temperature cycling stability of proton conductivity was tested (Fig. S26, ESI†). It can be seen from Fig. 3b that the proton conductivities at each temperature during the heating and cooling stages are not significantly different, suggesting its good temperature cycling stability in performance. Moreover, the E_a values of **D-UiO-66-N=IM** during the heating and cooling periods are also essentially consistent, indicating stable proton transport in **D-UiO-66-N=IM** (Fig. S27, ESI†). The time-dependent proton conductivities of **D-UiO-66-N=IM** at 70 °C and 100% RH were measured, from which it can be seen that it exhibits good durability in proton conductivity (Fig. 3c). Importantly, the results of PXRD patterns and FT-IR spectra of D-UiO-66-NH₂, UiO-66-N=IM, and **D-UiO-66-N=IM** after proton conductivity measurements show that they exhibit excellent structural stabilities, which is a crucial factor for practical applications (Fig. S28–S31, ESI†).

In conclusion, the **D-UiO-66-N=IM** with high proton conductivity of $2.15 \times 10^{-2} \text{ S cm}^{-1}$ at 70 °C and 100% RH was prepared using a dual strategy involving defect engineering and ligand modification. The findings indicate that the dual preparation strategy has a clear advantage compared to the single preparation strategy. This simple strategy offers various ideas for developing efficient proton conductors.

Xiao-Min Li: conceptualization, methodology, investigation, validation, writing – original draft, resources, writing – review & editing, funding acquisition. Junchao Jia: methodology, investigation, validation, writing – original draft, resources. Mingyang Zhao: investigation. Dongbo Liu: investigation. Junkuo Gao: supervision, funding acquisition, writing – review & editing. Ya-Qian Lan: supervision, writing – review & editing.

This work was supported by the project of the National Natural Science Foundation of China (No. 22301277), the Zhejiang Provincial Natural Science Foundation of China (No. LY20E020001), the Research Initiation Fund Project from Zhejiang Sci-Tech University (22212154-Y) and the Fundamental Research Funds of Zhejiang Sci-Tech University (No. 22212290-Y).

Data availability

The data supporting this article have been included as part of the ESI.†

Conflicts of interest

There are no conflicts to declare.

Notes and references

- 1 X.-M. Li and J. Gao, *SusMat*, 2022, 2, 504–534.
- 2 T. Wang, X. Ma, F. Chen, H. An, K. Chen and J. Gao, *Langmuir*, 2024, 40, 3873–3882.
- 3 W. Fang, W. Guo, R. Lu, Y. Yan, X. Liu, D. Wu, F. M. Li, Y. Zhou, C. He, C. Xia, H. Niu, S. Wang, Y. Liu, Y. Mao, C. Zhang, B. You, Y. Pang, L. Duan, X. Yang, F. Song, T. Zhai, G. Wang, X. Guo, B. Tan, T. Yao, Z. Wang and B. Y. Xia, *Nature*, 2024, 626, 86–91.
- 4 S. Y. Yi, E. Choi, H. Y. Jang, S. Lee, J. Park, D. Choi, Y. Jang, H. Kang, S. Back, S. Jang and J. Lee, *Adv. Mater.*, 2023, 35, 2302666.
- 5 S. Liu, Q. Meyer, Y. Li, T. Zhao, Z. Su, K. Ching and C. Zhao, *Chem. Commun.*, 2022, 58, 2323–2326.
- 6 M. Jouin, M. Bressel, S. Morando, R. Gouriveau, D. Hissel, M.-C. Péra, N. Zerhouni, S. Jemei, M. Hilairret and B. Ould Bouamama, *Appl. Energy*, 2016, 177, 87–97.
- 7 S. Ebrahimi, R. Roshandel and K. Vijayaraghavan, *Int. J. Hydrogen Energy*, 2016, 41, 22260–22273.
- 8 W.-L. Xie, X.-M. Li, J.-M. Lin, L.-Z. Dong, Y. Chen, N. Li, J.-W. Shi, J.-J. Liu, J. Liu, S.-L. Li and Y.-Q. Lan, *Small*, 2022, 18, 2205444.
- 9 G. J. Elfring and H. Struchtrup, *J. Membrane Sci.*, 2008, 315, 125–132.
- 10 G. Xu, A. Ke, G. Xu, Y. Liu, Y. Zuo, X. Yang, Y. Dong, J. Wang, J. Zheng, J. Li and W. Cai, *Int. J. Hydrogen Energy*, 2024, 56, 330–337.
- 11 J. Chen, Q. Mei, Y. Chen, C. Marsh, B. An, X. Han, I. P. Silverwood, M. Li, Y. Cheng, M. He, X. Chen, W. Li, M. Kippax-Jones, D. Crawshaw, M. D. Frogley, S. J. Day, V. García-Sakai, P. Manuel, A. J. Ramirez-Cuesta, S. Yang and M. Schröder, *J. Am. Chem. Soc.*, 2022, 144, 11969–11974.
- 12 J. Hu, H. Zhang, Z. Feng, Q.-R. Luo, C.-M. Wu, Y.-H. Zhong, J.-R. Li, L.-H. Chung, W.-M. Liao and J. He, *Chin. Chem. Lett.*, 2022, 33, 3227–3230.
- 13 D. Umeyama, S. Horike, M. Inukai, Y. Hijikata and S. Kitagawa, *Angew. Chem., Int. Ed.*, 2011, 50, 11706–11709.
- 14 J. Lee, D.-W. Lim, S. Dekura, H. Kitagawa and W. Choe, *ACS Appl. Mater. Interfaces*, 2019, 11, 12639–12646.
- 15 Y. Wang, Y. Lu, Z. Li, X.-W. Sun, W.-Y. Zhang, S. Zhang, J. Wang, T.-Y. Dang, Z. Zhang and S.-X. Liu, *Chem. Commun.*, 2021, 57, 8933–8936.
- 16 O. Basu, S. Mukhopadhyay, S. Laha and S. K. Das, *Chem. Mater.*, 2022, 34, 6734–6743.
- 17 Y. Ye, L. Gong, S. Xiang, Z. Zhang and B. Chen, *Adv. Mater.*, 2020, 32, 1907090.
- 18 F. Yang, G. Xu, Y. Dou, B. Wang, H. Zhang, H. Wu, W. Zhou, J.-R. Li and B. Chen, *Nat. Energy*, 2017, 2, 877–883.
- 19 X.-M. Li, J. Jia, D. Yang, J. Jin and J. Gao, *Chin. Chem. Lett.*, 2024, 35, 108474.
- 20 D.-W. Lim and H. Kitagawa, *Chem. Soc. Rev.*, 2021, 50, 6349–6368.
- 21 M. Kandiah, S. Usseglio, S. Svelle, U. Olsbye, K. P. Lillerud and M. Tilset, *J. Mater. Chem.*, 2010, 20, 9848–9851.
- 22 S.-Y. Zhu and B. Yan, *Dalton Trans.*, 2018, 47, 11586–11592.
- 23 Z. Sun, G. Li, H.-O. Liu and L. Liu, *Appl. Catal. A-Gen.*, 2013, 466, 98–104.
- 24 R. Kardanpour, S. Tangestaninejad, V. Mirkhani, M. Moghadam, I. Mohammadpoor-Baltork and F. Zadehahmadi, *J. Solid State Chem.*, 2015, 226, 262–272.
- 25 Y. Jiang, C. Liu, J. Caro and A. Huang, *Micropor. Mesopor. Mater.*, 2019, 274, 203–211.
- 26 M. J. Ingleson, J. Perez Barrio, J.-B. Guibaud, Y. Z. Khimyak and M. J. Rosseinsky, *Chem. Commun.*, 2008, 2680–2682.
- 27 Z. Sun, G. Li, H.-O. Liu and L. Liu, *Appl. Catal. A-Gen.*, 2013, 466, 98–104.
- 28 X. Ma, L. Wang, Q. Zhang and H.-L. Jiang, *Angew. Chem., Int. Ed.*, 2019, 58, 12175–12179.
- 29 G. C. Shearer, S. Chavan, J. Ethiraj, J. G. Vitillo, S. Svelle, U. Olsbye, C. Lamberti, S. Bordiga and K. P. Lillerud, *Chem. Mater.*, 2014, 26, 4068–4071.
- 30 G. C. Shearer, S. Chavan, S. Bordiga, S. Svelle, U. Olsbye and K. P. Lillerud, *Chem. Mater.*, 2016, 28, 3749–3761.
- 31 J. Jia, X.-M. Li, H. Wu, Q. Huang and J. Gao, *ACS Sustainable Chem. Eng.*, 2023, 11, 13502–13507.
- 32 S. J. Paddison, *Annu. Rev. Mater. Res.*, 2003, 33, 289–319.